

Context-Aware Timewise VAEs for Real-Time Vehicle Trajectory Prediction

Pei Xu, Jean-Bernard Hayet and Ioannis Karamouzas

Abstract—Real-time, accurate prediction of human steering behaviors has wide applications, from developing intelligent traffic systems to deploying autonomous driving systems in both real and simulated worlds. In this paper, we present ContextVAE, a context-aware approach for multi-modal vehicle trajectory prediction. Built upon the backbone architecture of a timewise variational autoencoder, ContextVAE employs a dual attention mechanism for observation encoding that accounts for the environmental context information and the dynamic agents’ states in a unified way. By utilizing features extracted from semantic maps during agent state encoding, our approach takes into account both the social features exhibited by agents on the scene and the physical environment constraints to generate map-compliant and socially-aware trajectories. We perform extensive testing on the nuScenes prediction challenge [1], Lyft Level 5 dataset [2] and Waymo Open Motion Dataset [3] to show the effectiveness of our approach and its state-of-the-art performance. In all tested datasets, ContextVAE models are fast to train and provide high-quality multi-modal predictions in real-time.

I. INTRODUCTION

Predicting human behaviors is crucial in the development of autonomous systems operating in human-populated spaces. Specifically, trajectory prediction for traffic agents is fundamental for the development of self-driving systems and intelligent traffic control systems. In this paper, we focus on the problem of trajectory prediction for vehicles in scenes populated with heterogeneous neighbors, including pedestrians, cyclists and other vehicles. Accurate trajectory prediction for such traffic agents requires the predictive model to fully take into account the external (observable) and internal (intentions) characteristics of the agents, in addition to the contextual influence from the agent’s neighbors and the scene environment.

Recently, variational autoencoder (VAE) architectures have been used for human trajectory prediction in homogeneous, human-human interaction settings, leading to state-of-the-art performance. Our work is in line with this family of predictive methods and builds upon the *timewise* variational autoencoder (VAE) trajectory prediction architecture introduced in [4]. The resulting SocialVAE approach has been shown to effectively capture human-human interactions in complex scenarios and achieve state-of-the-art performance on several benchmarks of human trajectory prediction. However, it only considers agent

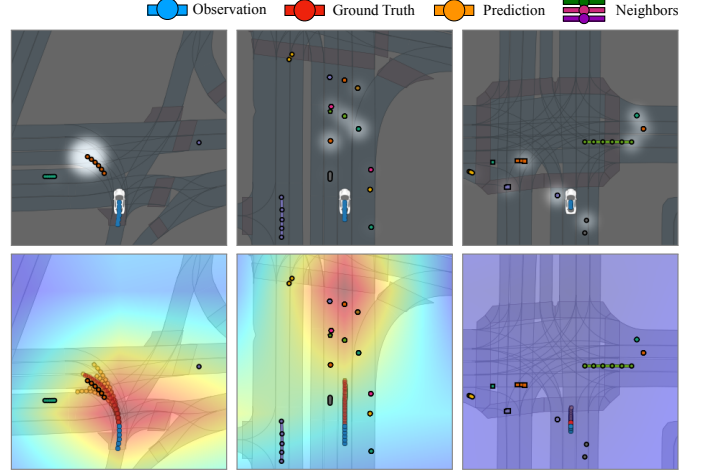


Fig. 1. Trajectory predictions on the Lyft dataset using our proposed approach. ContextVAE employs a timewise VAE architecture and a context-aware observation encoding scheme that accounts for environmental (map) and social (neighbor) features in a unified manner. Top: Corresponding attention that the target vehicle is paying to its neighbors within a radius of 30m. Bottom: Predicted trajectories and map regions with high activation in the attention model. Red regions are considered more visually salient than blue regions. The white car identifies the vehicle agent under prediction. Observed trajectories are shown in blue, and the ground-truth future trajectories are shown in red. Other colored dots and lines denote stationary and moving neighbors respectively. Light red polygons on the map denote crosswalks.

states as the input for trajectory prediction and ignores the influence from the environmental context on the agent’s steering decision making. This limits its applicability on vehicle trajectory prediction tasks, where the environmental context (roads, lanes, etc.) is critical to generate map-compliant trajectories.

In this paper, we introduce ContextVAE as a novel approach for vehicle trajectory prediction. While keeping a timewise VAE architecture [4], ContextVAE adopts a dual attention mechanism for observation encoding, which simultaneously takes into account the environmental context extracted from the map features and the social context extracted from the neighboring agents’ states. Previous VAE-based works for vehicle trajectory prediction employ a *decoupled* observation encoding scheme, where environmental and social contexts are encoded separately and then are simply concatenated to produce the final encoding used for prediction [5]–[8]. In contrast, we propose to encode the environmental and social contexts in a *unified* way, based on the intuition that humans account for environmental features dynamically and instantaneously during navigation decision making, rather than using such features to evaluate different navigation paths after the fact. Instead of directly plotting trajectories on raster-

* This work was supported by the National Science Foundation under Grant No. IIS-2047632 and by an unrestricted gift from Roblox.

Pei Xu and Ioannis Karamouzas are with the School of Computing at Clemson University, South Carolina, USA. {peix, ioannis}@clemson.edu

Jean-Bernard Hayet is with the Department of Computer Science at CIMAT, A.C., Mexico. jbhayet@cimat.mx

ized maps, our approach uses an RNN-based encoding of the perceived neighbors along with the extracted local map features as the context for encoding the local state of the agent under prediction. As such, we avoid processing a sequence of rasterized maps for faster inference. Meanwhile, the extracted environmental features directly participate in the agent's state encoding process, leading to a fully, context-aware scheme for observation encoding that allows for a better inference of an agent's navigation strategy.

We demonstrate the effectiveness of our proposed ContextVAE and its underlying encoding scheme on vehicle trajectory prediction tasks from large-scale, heterogeneous datasets including the nuScenes prediction challenge [1], Lyft Level 5 dataset [2] and Waymo Open Motion Dataset [3]. As shown in Fig. 1, our approach accurately captures the relevant map features to generate map-compliant trajectories while simultaneously taking into account the nearby traffic agents and the self-state of the agent under prediction. Since our approach works directly with vectorized map features and agent states, it can provide multi-modal predictions in real-time. We show that our approach's performance is rather insensitive to the nature of the employed map feature extraction module. Overall, models trained with ContextVAE lead to state-of-the-art performance on the tested datasets. They are fast to train, have a small memory footprint, and provide high-quality multi-modal predictions in real-time.

II. RELATED WORK

Leveraging environmental context: To produce map-compliant predictions, early works directly plot the observed trajectories (agent of interest and neighbors) on the rasterized scene maps, performing prediction mainly by using convolutional neural networks (CNNs) to extract map features without fully exploiting the agent states like velocity and acceleration [2], [9]–[11]. More recent works exploit both the environmental context and vectorized neighbors' states as inputs to the prediction model for the sake of better synthesizing the agent's motion states and context [6], [7], [9], [12]–[17]. Beyond rasterized maps, some approaches leverage the graph representation of high-definition (HD) maps to avoid information loss during rasterization [18], [19]. Systems such as VectorNet [18] and AutoBots [14] have shown that CNNs applied on rasterized maps can be replaced by graph neural networks (GNNs) using graph-represented maps as the input without changing the prediction model's overall architecture.

Generating sequential predictions: CoverNet [9] and MultiPath [11], as early works, generate trajectories by picking them from a predefined trajectory set and convert the generative task to a classification problem. WIMP [20], Trajectron++ [6] and DiversityGAN [16] leverage recurrent neural networks (RNNs) to perform prediction sequentially. MTP [12], AutoBots [14] and LaPred [21] output fixed-length predicted trajectories at once. WIMP [20], CXX [22], TNT [23], GoalNet [15] and SGNet [17] first predict goal positions and then generate trajectories between the agent's last observed position and the predicted goals. IMA [5] and M2I [24], instead of predicting trajectories only for target agents, perform prediction

sequentially for all the agents. P2T [13] and PGP [25] take a reinforcement learning approach, with a reward-based model upon which a policy is trained to perform prediction. P2T uses a goal-directed way to generate trajectories and PGP generates paths by traversing nodes in the road graph.

Handling multi-modality: To model the uncertainty during human driving and account for multi-modal decision making, Trajectron++ [6], BiTrap [7] and SGNet [17] exploit a conditional variational autoencoder (CVAE) architecture where the prior on the latent variable is modeled as a mixture of Gaussians. AutoBots [14] uses Gaussian mixtures as well but considers an encoder-decoder architecture without variational inference. DiversityGAN [16] takes the architecture of generative adversarial networks to produce stochastic results. LaPred [21] employs K blocks of fully connected layers with random initialization to produce K predictions parallelly. P2T [13] and PGP [25] rely on a discrete policy under the framework of reinforcement learning to make predictions.

Introducing prior knowledge: Besides leveraging vectorized HD maps, recent works introduce prior knowledge [26] into the process of vehicle trajectory prediction. For example, CXX [22], WIMP [20], P2T [13], LaPred [21], LaneR-CNN [27] and GOHOME [28] select interesting paths traversing the road graph or specific lanes in the graph as the basis to generate numeric coordinates. TNT [23] and GoalNet [15] select goal positions based on the road graph and then perform goal-directed prediction. Though achieving impressive results on some benchmarks, such approaches heavily rely on the assumption that vehicles will move between nodes in the road graph or along specific lanes, which is not always true in real-life scenarios. In this work, therefore, we focus on comparison with works that do not rely on this assumption.

III. APPROACH

A. Problem Formulation

Given a local, T -frame observation $\mathcal{O}_i^{1:T}$ gathered from a target agent i , we seek to estimate the agent's trajectory predictive distribution over the future H frames, i.e. $p(\mathbf{x}_i^{T+1:T+H}|\mathcal{O}_i^{1:T})$, where $\mathbf{x}_i^{T+1:T+H}$ are the agent's future position coordinates from frame $T+1$ to frame $T+H$. To perform context-aware prediction, we consider observations that include both the N_i observed neighboring agent states (positions) and environmental context information, i.e. $\mathcal{O}_i^t := \{\mathbf{M}_i^t, \{\mathbf{x}_j^t\}_{j=1}^{N_i}\}$, where $j = 1, \dots, N_i$ and $\|\mathbf{x}_j^t - \mathbf{x}_i^t\| \leq r_i$ given r_i as the observation radius of agent i . \mathbf{M}_i^t is a representation of the local environmental context, that we model as a vector of features extracted from rasterized semantic maps via a CNN module, as shown in Fig. 2. To train our models in a scene-invariant way, we do not predict directly the global coordinates $\mathbf{x}_i^{T+1:T+H}$ but rather the *displacement* distribution $p(\mathbf{d}_i^{T+1:T+H}|\mathcal{O}_i^{1:T})$, where $\mathbf{d}_i^t := \mathbf{x}_i^t - \mathbf{x}_i^{t-1}$ is the displacement between two frames. Future trajectories are reconstructed as $\mathbf{x}_i^{T+\tau} = \mathbf{x}_i^T + \sum_{t=T+1}^{T+\tau} \mathbf{d}_i^t$ by sampling \mathbf{d}_i^τ from the predicted distributions.

In the following, we present our proposed ContextVAE approach for context-aware trajectory prediction.

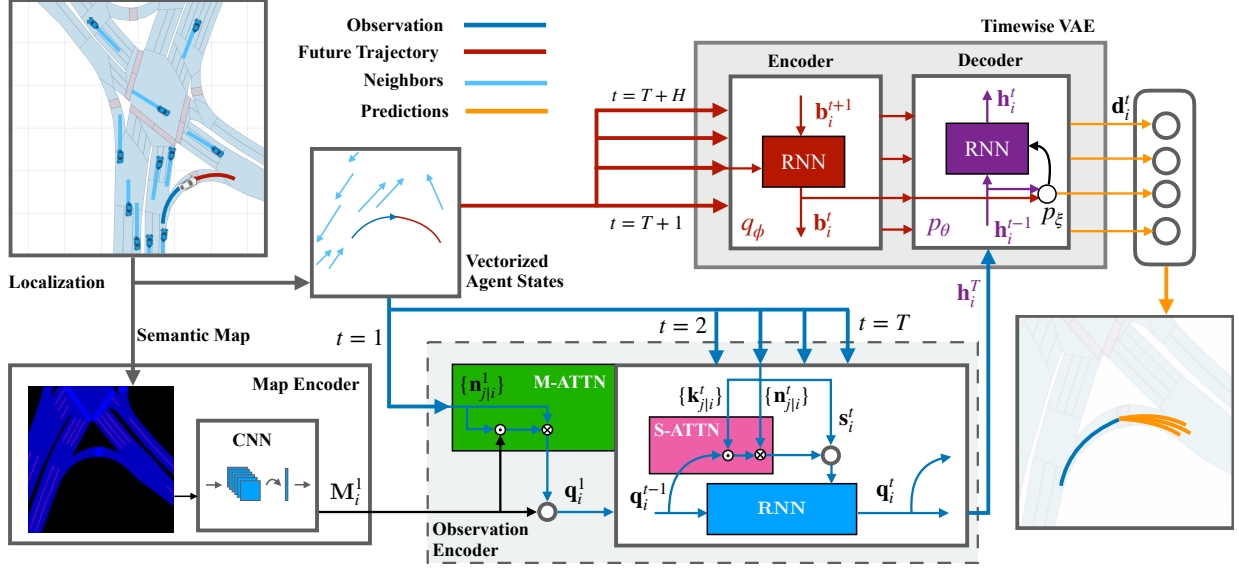


Fig. 2. System overview of ContextVAE for vehicle trajectory prediction. Our approach’s backbone architecture is a timewise VAE shown in the gray block at the upper right. The proposed map encoding module is linked to the backbone timewise VAE architecture through the context-aware observation encoder (dashed box), which processes the vectorized agent states in a unified way with the map features. M-ATTN and S-ATTN represent the map and social attention respectively, where \odot represents the dot product operator, \otimes represents the element-wise multiplication operator, and \circ represents the concatenation operator. Red parts for posterior estimation are used only during training.

B. Model Architecture and Training Objective

The backbone architecture of ContextVAE is a timewise VAE with a conditional prior p_θ and a posterior q_ϕ estimated bidirectionally (see Fig. 2). The training objective is to maximize a timewise evidence lower bound:

$$\mathbb{E}_i \left[\frac{1}{H} \sum_{t=T+1}^{T+H} \mathbb{E}_{\mathbf{z}_i^t \sim q_\phi(\cdot | \mathbf{b}_i^t, \mathbf{h}_i^{t-1})} \left[\log p_\xi(\mathbf{d}_i^t | \mathbf{z}_i^t, \mathbf{h}_i^{t-1}) - D_{KL} [q_\phi(\mathbf{z}_i^t | \mathbf{b}_i^t, \mathbf{h}_i^{t-1}) || p_\theta(\mathbf{z}_i^t | \mathbf{h}_i^{t-1})] \right] \right], \quad (1)$$

where \mathbf{z}_i^t is the latent variable sampled timewise, and \mathbf{b}_i^t and \mathbf{h}_i^{t-1} are the RNN hidden states, which are updated backward in the encoder and forward in the decoder, respectively. We parameterize the output distribution p_ξ , the posterior q_ϕ and the prior p_θ as Gaussians, using neural networks.

The timewise VAE decoder hidden state \mathbf{h}_i^t for $t > T$ is updated recurrently based on the sampled \mathbf{z}_i^t and the displacement \mathbf{d}_i^t , i.e. $\mathbf{h}_i^t = \vec{g}(\psi_{\mathbf{z}\mathbf{d}}(\mathbf{z}_i^t, \mathbf{d}_i^t), \mathbf{h}_i^{t-1})$. The initial state \mathbf{h}_i^T encodes the observation via $\mathbf{h}_i^T = \psi_{\mathbf{h}}(\mathcal{O}_i^{1:T})$, where $\psi_{\mathbf{z}\mathbf{d}}$ and $\psi_{\mathbf{h}}$ are embedding networks. This leads to a prior conditioned by the context observation $\mathcal{O}_i^{1:T}$ (see III-C). The timewise VAE encoder hidden state \mathbf{b}_i^t is updated backwards, i.e. $\mathbf{b}_i^t = \overleftarrow{g}(\mathcal{O}_i^t, \mathbf{b}_i^{t+1})$, given the ground-truth observation \mathcal{O}_i^t at the future frame $t > T$ and a zero initial state \mathbf{b}_i^{T+H+1} .

This way, during training, the output distribution p_ξ relies on the latent variable \mathbf{z}_t drawn from the backward posterior $q_\phi(\cdot | \mathbf{b}_i^t)$ and \mathbf{h}_{t-1} given by the forward prior p_θ , and thus uses features provided by the whole trajectory $\mathcal{O}_i^{1:T+H}$ for better extracting the agent’s navigation strategy. At inference, predictions are generated through latents drawn from the prior sequentially: $\mathbf{d}_i^t \sim p_\xi(\cdot | \mathbf{z}_i^t, \mathbf{h}_i^{t-1})$ where $\mathbf{z}_i^t \sim p_\theta(\cdot | \mathbf{h}_i^{t-1})$, thereby relying on the historical observation $\mathcal{O}_i^{1:T}$ only.

C. Context-Aware Observation Encoding

for observation encoding, where the environmental context extracted from the semantic map and the social context extracted from the observed agent states are exploited simultaneously. Our scheme leverages a dual attention mechanism that combines *map attention* with *social attention* as shown at the bottom of Fig. 2.

Following prior literature [4], [6], [7], [29], our observation encoder employs an RNN structure g (blue box in Fig. 2) that encodes the agent state sequentially. The RNN is updated as

$$\mathbf{q}_i^{t+1} = g(\mathcal{O}_i^t, \mathbf{q}_i^t), \quad (2)$$

where, from the local observation \mathcal{O}_i^t , we use the agent’s self states \mathbf{s}_i^t , including the agent’s velocity and acceleration, and the observed neighbors’ state $\{\mathbf{n}_{j|i}^t\}$, including the relative position and velocity of each neighbor j to the agent i . The final \mathbf{q}_i^T is used to initialize the decoder’s hidden states in the timewise VAE backbone, i.e., $\psi_{\mathbf{h}}(\mathcal{O}_i^{1:T}) \equiv \mathbf{q}_i^T$ (Section III-B).

To account for how the environmental context influences the agent’s steering actions, we propose to initialize the hidden state \mathbf{q}_i^1 using features extracted from the local semantic map, rather than encode the map and the agent’s state independently. However, instead of directly plugging the map features into the observation encoder, we introduce a *map attention* (M-ATTN) mechanism and initialize the encoder via

$$\mathbf{q}_i^1 = \text{CONCAT} \left(\mathbf{M}_i^1, \text{M-ATTN}(\{\mathbf{n}_{j|i}^1\}) \right), \quad (3)$$

where

$$\begin{aligned} \text{M-ATTN}(\{\mathbf{n}_{j|i}^1\}) &\triangleq \text{ATTN}(\mathbf{M}_i^1, \{\mathbf{n}_{j|i}^1\}, \{\mathbf{n}_{j|i}^1\}) \\ &= \sum_j w_{j|i} f_{\mathbf{n}_{\text{val}}}(\mathbf{n}_{j|i}^1). \end{aligned} \quad (4)$$

Here, \mathbf{M}_i^1 denotes vectorized features extracted from agent i ’s local map at the *first* observation frame, and f_{\cdot} are

embedding networks. \mathbf{M}_i^1 , $\{\mathbf{n}_{j|i}^1\}$ and $\{\mathbf{n}_{j|i}^1\}$ correspond to the query, key, and value vectors, respectively, of the attention mechanism. The attention weights $w_{j|i}$ are obtained through dot-product operation between \mathbf{M}_i^1 and $\mathbf{n}_{j|i}^1$ followed by a softmax operation, i.e.

$$w_{j|i} = \frac{\exp\left(f_{\mathbf{M}^1}(\mathbf{M}_i^1) \odot f_{\mathbf{n}_{\text{key}}}(\mathbf{n}_{j|i}^1)\right)}{\sum_{j' \neq i} \exp\left(f_{\mathbf{M}^1}(\mathbf{M}_i^1) \odot f_{\mathbf{n}_{\text{key}}}(\mathbf{n}_{j'|i}^1)\right)}. \quad (5)$$

The resulting M-ATTN mechanism can help identify neighbors that are located nearby the target agent but have less influence in the given context, e.g., vehicles that are spatially close to the agent but drive on a lane that is inaccessible to it. We refer to Section IV-E and Fig. 1 for related qualitative results and to Section IV-C for a quantitative analysis.

During agent state encoding, we synthesize the social context represented by the neighbors' states $\{\mathbf{n}_{j|i}^t\}$ via a *social attention* (S-ATTN) mechanism as:

$$\begin{aligned} \text{S-ATTN}(\{\mathbf{n}_{j|i}^t\}) &\triangleq \text{ATTN}(\mathbf{q}_i^t, \{\mathbf{k}_{j|i}^t\}, \{\mathbf{n}_{j|i}^t\}) \\ &= \sum_j \omega_{j|i} f_{\mathbf{n}_{\text{val}}}(\mathbf{n}_{j|i}^t), \end{aligned} \quad (6)$$

where, \mathbf{q}_i^t , $\{\mathbf{k}_{j|i}^t\}$, and $\{\mathbf{n}_{j|i}^t\}$ correspond to the query, key and value vectors of the attention, and each weight $\omega_{j|i}$ of the attention graph is computed as the dot product between \mathbf{q}_i^t and $\mathbf{k}_{j|i}^t$ after obtaining their fixed-length embeddings. Here, $\mathbf{k}_{j|i}^t$ denotes the social features exhibited by the neighbor j and observed by the agent i . As introduced in [4], [29], we include the distance, bearing angle and minimal predicted distance from agent i to j as the social features $\mathbf{k}_{j|i}^t$.

By choosing a proper size of the local map, we can have \mathbf{M}_i^1 covering the whole trajectory of the agent during the observation and prediction horizon from $t = 1$ to $t = T + H$. This allows us to sidestep introducing \mathbf{M}_i^1 timewisely, and update the hidden state in Eq. 2 by representing \mathcal{O}_i^t as

$$\mathcal{O}_i^t \equiv \text{CONCAT}\left(\mathbf{s}_i^t, \text{S-ATTN}(\{\mathbf{n}_{j|i}^t\})\right). \quad (7)$$

This way, we perform fast observation encoding directly on the environmental and social contexts after just one pass of the map encoding module, and avoid the computationally expensive processing a sequence of rasterized maps. We refer to Section IV-C for our model's real-time prediction performance.

As shown in Fig. 2, we exploit rasterized semantic maps to capture contextual information and extract the related features \mathbf{M}_i^1 using a CNN module. However, we note that there is no constraint about the form of \mathbf{M}_i^1 . For example, \mathbf{M}_i^1 can also be represented using graphs processed by a GNN [18], [19], [23], [25], [28], or using a lane attention block [21], [22]. Since map rasterization is the common way to generate semantic maps for contextual information and given that most open-source vehicle datasets do not provide an API to directly generate road graphs, in our experiments we rely on CNNs to extract contextual features from rasterized maps.

IV. EXPERIMENTS

We evaluate our approach on vehicle trajectory prediction tasks using the nuScenes prediction challenge (*nuScenes*) [1],

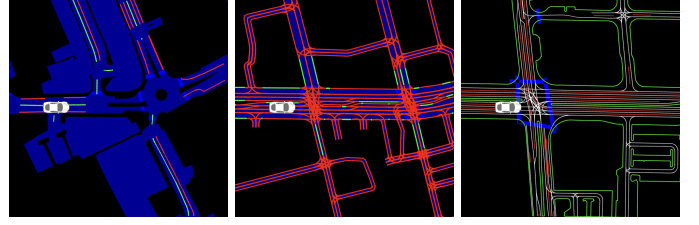


Fig. 3. Examples of rasterized semantic maps for each dataset. From left to right: *nuScenes*, *Lyft* and *Waymo*. Blue identifies drivable areas and crosswalks; green identifies road edges; red identifies lane dividers. In the *Waymo* maps, we enhance the drivable area with lane center lines colored in white. The drawn cars identify the first observed position of the agent under prediction, which also indicates the map's local origin and x -axis direction. The cars are not part of the rasterized maps.

Lyft Level 5 Prediction Dataset (*Lyft*) [2] and *Waymo* Open Dataset (*Waymo*) [3]. These datasets handle heterogeneous types of agents, including various vehicles, cyclists, pedestrians. We focus our prediction on vehicles' trajectories and all other types of agents are considered as neighbors.

A. Setup

a) *Implementation details*: We use a rasterized, 224×224 local semantic map to represent the environmental context. The map is translated and rotated such that the vehicle under prediction heads towards the positive x -axis and stands at the 122nd row and 51st column of the map in the 1st frame of observation. To be consistent, the coordinates of all agents are expressed using the same local system. Fig. 3 shows examples of the extracted maps for the three datasets. Since each dataset has its own semantic map definition, the generated rasterized maps are slightly different. We refer to the supplementary material for details on semantic map rasterization.

b) *Evaluation Metrics and Baselines*: We use the minimum average displacement error over k predictions (minADE_k) and the minimum final displacement error over k predictions (minFDE_k) to assess a model's performance. We consider both the most likely prediction ($k = 1$) and the top-5 predictions ($k = 5$) as our key metrics measured in meters. We provide comparisons to two deterministic baselines: *Constant Velocity* assumes target vehicles always move at the velocity defined between the last two observed frames; *Kalman Filter* applies an extended Kalman filter while assuming constant longitudinal speed and heading direction. We also consider state-of-the-art, data-driven baselines for each dataset. Since our approach does not use prior knowledge to constrain the movement of vehicles, we limit our comparison to approaches without restricting the accessibility of vehicles via maps or refining predicted trajectories at a post-processing stage.

B. Quantitative Results

a) *nuScenes*: We use the official training and validation sets of *nuScenes* prediction challenge to perform model training and performance evaluation. An observation window of up to 2s is used and the prediction horizon is 6s. As the data was recorded at 2FPS, this leads to a 12-frame prediction and a varying observation window between 2 and 5 frames. Additionally to *Constant Velocity* and *Kalman Filter*, we introduce

TABLE I
PERFORMANCE ON NUSCENES PREDICTION CHALLENGE.

<i>nuScenes</i> (Validation Set)	minADE _k (m)		minFDE _k (m)	
	<i>k</i> = 1	<i>k</i> = 5	<i>k</i> = 1	<i>k</i> = 5
Constant Velocity	4.61	-	11.21	-
Kalman Filter	4.17	-	10.99	-
Trajectron++	4.08	2.41	9.67	5.63
P2T	3.82	1.86	8.95	4.08
AutoBots-Ego	3.86	1.70	8.89	3.40
ContextVAE	3.54	1.59	8.24	3.28

TABLE II
PERFORMANCE ON LYFT LEVEL 5 PREDICTION DATASET.

<i>Lyft</i>	minADE _k (m)		minFDE _k (m)	
	<i>k</i> = 1	<i>k</i> = 5	<i>k</i> = 1	<i>k</i> = 5
Constant Velocity	0.70	-	1.64	-
Kalman Filter	0.60	-	1.30	-
SAMPP [5]	0.39	-	0.83	-
IMAP [5]	0.28	-	0.65	-
Trajectron++	0.38	0.26	0.89	0.57
ContextVAE	0.24	0.16	0.54	0.32

three other baselines for comparison. The Trajectron++ [6] model is trained from scratch with two known bugs fixed as indicated in the official repository. P2T [13] is tested using their provided pre-trained model. Since no pre-trained models are provided, we train the AutoBots-Ego model using the official implementation. These three baselines exploit CNN modules for map encoding. We report the results in Table I. Among the considered baselines, *Constant Velocity* and *Kalman Filter* perform the worst. As recently published works, P2T and AutoBots-Ego work significantly better than Trajectron++, with AutoBots-Ego outperforming P2T. However, its training is very time-consuming. AutoBots-Ego needed more than three days to perform 70-epochs training using a V100 GPU, despite the fact that *nuScenes* has only 32,186 trajectories for training. Our approach not only achieves the best performance on all four metrics, but it is also extremely fast to train, needing only about 2 hours to train on a single V100 GPU.

b) Lyft: This dataset is much larger than *nuScenes* and has more than 1,000 hours of data with 170,000 scenes. We use only the first 16,265 scenes of the training data, with each scene being about 24s long. For evaluation, we use the full validation dataset (16,220 scenes). We downsample the data from 10FPS to 5FPS and train models with an observation window of 1s and prediction horizon of 3s. In Table II, we report the performance obtained by our approach and two newly introduced baseline models: SAMPP and IMAP [5]. These are deterministic models that rely on lane graphs rather than rasterized semantic maps. They use the same observation window and prediction horizon as ours, and we list their reported numbers in the table. Trajectron++ is introduced as a multimodal baseline, trained using the same data as ours. As it can be seen, IMAP achieves better deterministic results (minADE₁/minFDE₁) compared to Trajectron++, though these results are slightly worse compared to Trajectron++’s multimodal performance. Our approach outperforms IMAP and Trajectron++ on both the deterministic and multimodal results,

TABLE III
PERFORMANCE ON WAYMO OPEN DATASET.

<i>Waymo</i> (Validation Set)	minADE _k (m)		minFDE _k (m)	
	<i>k</i> = 1	<i>k</i> = 5	<i>k</i> = 1	<i>k</i> = 5
Constant Velocity	2.04	-	5.25	-
Kalman Filter	1.99	-	4.07	-
SAMPP [5]	1.26	-	2.80	-
IMAP [5]	0.97	-	2.03	-
Trajectron++	0.88	0.56	2.37	1.41
MotionCNN	0.83	0.40	1.99	0.81
M2I	0.67	0.42	1.60	0.85
ContextVAE	0.59	0.30	1.49	0.68

with an improvement around 15% on minADE₁/minFDE₁ and around 40% on minADE₅/minFDE₅.

c) Waymo: This dataset has two types of training data formats, consisting of 20s and 9s sequential data, respectively. We use the 9s data for training, which contains 487,002 scenes, while the validation set has 44,097 scenes. In addition to performing downsampling from 10FPS to 5FPS, we apply the data filter from the *Lyft* dataset to filter out invalid data. Similar to our *Lyft* implementation we use a 1s window for observation and a 3s horizon for prediction. Following the Waymo motion prediction challenge design, we train and evaluate our model using only the vehicle agents labeled as objects of interest. Table III shows the performance of our approach along with two new baselines: MotionCNN [10] and M2I [24]. We run the pre-trained models from the two baselines and keep the first 3s prediction for evaluation. As shown in Table III, MotionCNN and M2I outperform Trajectron++ with a significant improvement on minADE₅/minFDE₅. M2I also brings a large improvement on the most likely prediction. Compared with these two strong baselines, our approach achieves more than 15% improvement overall, and a 29% and 20% improvement on minADE₅ and minFDE₅, respectively.

The default Waymo motion prediction challenge setup uses an 8s prediction horizon with *k* = 6. The performance of our model trained for 8s prediction on the *interactive* validation set is: minADE₆ = 1.59 and minFDE₆ = 3.67. As a comparison, the Waymo LSTM baseline achieves minFDE₆ = 6.07 for 8s prediction [30], and M2I [24] reports minFDE₆ = 5.49.

C. Sensitivity Analysis

a) CNN Modules: We evaluated the performance of ContextVAE with several popular CNN modules for map encoding. In Table IV, we report the corresponding results along with the number of parameters and inference time taken by each CNN module. The inference time refers to the time needed to perform *k* = 5 predictions for one batch of 512 input samples. The reported time is measured on a machine equipped with a V100 GPU and averaged over 10,000 test trials. As can be seen in the table, there are no large differences regarding minADE_k/minFDE_k among the tested CNN modules on *Lyft* and *Waymo*. We can therefore safely choose a small module, like EfficientNet-B0 or MobileNet-V2, for the sake of faster inference. In *nuScenes*, the best performance is obtained with ResNet18, but the differences among the CNN modules are larger. A possible reason is the small size of the *nuScenes*

TABLE IV
PREDICTION ERRORS WITH DIFFERENT CNN MODULES FOR MAP FEATURE EXTRACTION.

CNN Module	Infer. Time	# of Params.	<i>nuScenes</i>				<i>Lyft</i>				<i>Waymo</i>			
			minADE _k (m)		minFDE _k (m)		minADE _k (m)		minFDE _k (m)		minADE _k (m)		minFDE _k (m)	
			k = 1	k = 5	k = 1	k = 5	k = 1	k = 5	k = 1	k = 5	k = 1	k = 5	k = 1	k = 5
ResNet18	0.23s	11.7M	3.543	1.586	8.244	3.277	0.247	0.165	0.548	0.324	0.600	0.306	1.532	0.709
ResNet152	1.33s	60.2M	3.728	1.728	8.773	3.657	0.244	0.164	0.544	0.321	0.598	0.306	1.530	0.708
EfficientNet-B0	0.25s	5.3M	3.715	1.740	8.733	3.676	0.246	0.165	0.548	0.325	0.585	0.299	1.491	0.686
MobileNet-V2	0.20s	3.5M	3.780	1.738	8.888	3.671	0.251	0.165	0.560	0.321	0.585	0.298	1.492	0.684

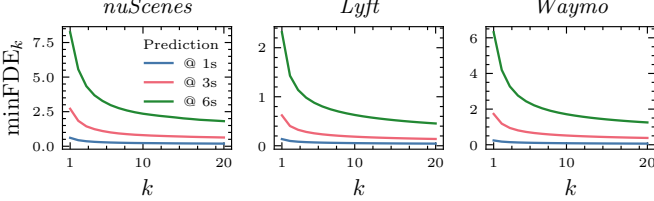


Fig. 4. Minimal final displacement error (in meters) as a function of the number k of predicted trajectories for different prediction horizons.

dataset, which makes the model more sensitive to the choice of CNN modules. Overall, using ResNet18 on *nuScenes* meets the real-time inference requirements while guaranteeing high prediction accuracy. For a complete list of all the tested CNN modules, we refer to the supplementary material.

b) *Prediction Horizon and Choice of k* : Intuitively, increasing the prediction horizon leads to more uncertainty, making prediction harder. This is consistent with results shown in Fig. 4, where larger horizons lead to higher minFDE values. For a given horizon, an important question is how many prediction samples k are enough to lead to a sufficiently low error? For a 1s prediction horizon (blue line), the error converges around $k = 10$. For a 3s horizon (red line), $k = 20$ roughly leads to convergence. However, for a 6s horizon (green line), there is still a decreasing trend at $k = 20$. We refer to the supplementary material for more numeric results of model performance with different prediction horizons.

c) *Ablation Study*: In Table V, we perform ablation studies on *Waymo*, related to our proposed unified observation encoding scheme and its underlying dual attention mechanism (M-ATTN in Eq. 4 and S-ATTN in Eq. 6). When neither map nor social context is exploited, the neighbors' states are simply added together for observation encoding, i.e. $\mathcal{O}_i^t \equiv \text{CONCAT}(\mathbf{s}_i^t, \sum_j f_n(\{\mathbf{n}_{j|i}^t\}))$ instead of Eq. 7. When only S-ATTN is used, the observation encoder is initialized as $\mathbf{q}_i^1 = \sum_j f_{n^1}(\mathbf{n}_{j|i}^1)$ instead of Eq. 3. When the map is introduced independently ("Indie"), \mathbf{q}_i^1 is initialized similarly to S-ATTN and the output \mathbf{q}_i^T of the encoder is concatenated with the map features \mathbf{M}_i^1 to provide the initial state for the time-wise VAE decoder, i.e. $\mathbf{h}_i^T \equiv \text{CONCAT}(\mathbf{q}_i^T, \mathbf{M}_i^1)$. In contrast, in our proposed observation encoding scheme, the map features are integrated into the encoder ("Integrated"), with \mathbf{M}_i^1 being used for initializing \mathbf{q}_i^1 and $\mathbf{h}_i^T \equiv \mathbf{q}_i^T$. This allows for map and agents' states to be encoded in a unified manner. When M-ATTN is employed, \mathbf{q}_i^1 is initialized as shown in Eq. 3. Without M-ATTN, we simply integrate the map features and the agent's neighbors as $\mathbf{q}_i^1 = \text{CONCAT}(\mathbf{M}_i^1, \sum_j f_{n^1}(\{\mathbf{n}_{j|i}^1\}))$. As can be seen from Table V, S-ATTN brings about 4% im-

TABLE V
MODEL ABLATION ON *Waymo*.

S-ATTN	MAP	M-ATTN	minADE _k (m)		minFDE _k (m)	
			k = 1	k = 5	k = 1	k = 5
-	-	-	0.68	0.45	1.78	1.11
✓	-	-	0.65	0.43	1.71	1.06
✓	Indie	-	0.63	0.37	1.68	0.85
✓	Integrated	-	0.62	0.33	1.65	0.70
✓	Integrated	✓	0.59	0.30	1.49	0.68

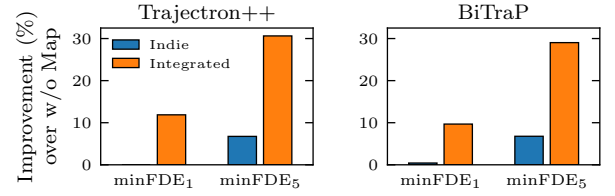


Fig. 5. Performance improvement when using map context on *Waymo* dataset.

provement over the basic timewise VAE backbone. Handling the semantic map independently from the social context brings an extra 3% improvement on the deterministic predictions and around 15% on the multimodal predictions. Integrating the map into the encoder without M-ATTN results in even better performance, highlighting its potential over Indie maps. M-ATTN further boosts the performance with an improvement around 35% on minADE₅/minFDE₅, and around 15% on minADE₁/minFDE₁ compared to the basic backbone architecture. Similar conclusions can be drawn from the *nuScenes* and *Lyft* datasets, as described in the supplementary material.

D. Integrated vs. Independent Maps for Observation Encoding

To further highlight the effectiveness of using Integrated rather than Indie maps for RNN-based observation encoding, we consider experiments with additional VAE-based approaches that by default decouple environmental context from social context. Fig. 5 compares the performance of Trajectron++ [6] when Indie maps and Integrated maps are employed to its performance when no semantic maps are used. The Indie scheme follows the original implementation of Trajectron++ that accounts for map features independently from the agents' states. In the Integrated model, the map features are used to initialize the RNN hidden state of the observation encoder. We also extend the BiTraP [7] method to work with rasterized maps by using the same map encoding module as Trajectron++ and report the related comparisons in the figure. As can be seen, models with Integrated maps significantly improve the performance of Trajectron++ and Bitrap on both deterministic and multimodal predictions. In contrast, Indie maps do not

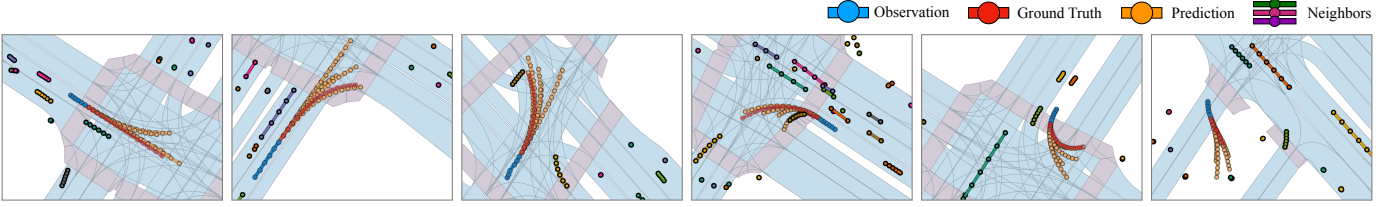
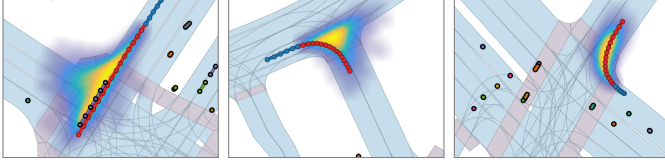


Fig. 6. Qualitative examples from *Lyft*. Observed trajectories are shown in blue. The ground-truth future trajectories are shown in red. 5 predictions are shown in orange. Other colored dots and lines denote stationary and moving neighbors respectively.

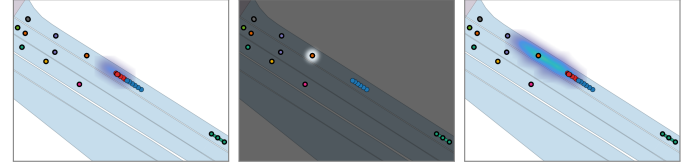
Prediction with S-ATTN + M-ATTN



Prediction with S-ATTN

Social Attention Map

Prediction w/o S-ATTN



Prediction w/o Map (S-ATTN only)

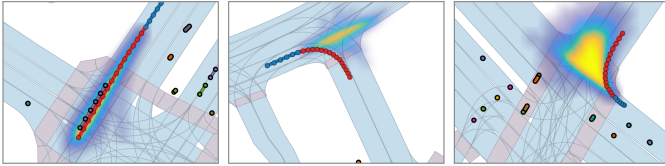


Fig. 7. Case studies with (top) and without (bottom) considering rasterized maps in the observation encoder. The trajectory distributions heatmaps are generated using 2,000 predictions.

provide any noticeable performance gain on deterministic predictions and only bring a small improvement on multimodal ones. We refer to the supplementary material for complete results on all the tested datasets.

E. Case Studies

Fig. 6 shows predictions obtained with ContextVAE on the *Lyft* dataset. As can be seen, using maps makes the model aware of the lanes and results in covering the ground-truth trajectories closely, while also accounting for other possible driving maneuvers that could be taken. In the first three scenes, for example, ContextVAE accurately assigns samples to different lanes at the multi-lane intersections. In the fourth scene, the model predicts the target vehicle’s turning-left behavior along with a potential U-turn behavior. The last two cases exemplify non map-compliant behaviors, where the vehicle drives from and to the off-map region, respectively. While graph-based methods typically struggle with off-road cases, our approach accurately predicts the vehicles’ movement.

In Fig. 7, we highlight additional examples comparing the prediction results of ContextVAE to the results obtained when the map and its related attention mechanism are disabled from the observation encoder. Ignoring maps can lead to myopic as well as wrong predictions. In the first two cases, for example, the model predicts that the target vehicle will keep driving straight and does not account for the multi-modal decisions at intersections. While in the third scene, the model predicts multi-modal driving trajectories, such trajectories are invalid as the vehicle can only take a right turn. In contrast, accounting for map attention leads to map-compliant paths and helps to predict potential turning behaviors at intersections.

Fig. 8. Case study from *Lyft* with/without accounting for S-ATTN in observation encoding. The left and middle figures show the heatmap of the predicted trajectory distribution and the social attention of the target vehicle, respectively, given neighbors observed within a radius of 30m. The right figure shows the predictions without using the S-ATTN mechanism, i.e., ignoring the pink box from the observation encoder in Fig. 2.

As discussed in the ablation study, the social attention mechanism of the observation encoder is equally important, allowing the model to infer the interactions between agents in the scene. Fig. 8 depicts an indicative example where ContextVAE performs prediction with and without using the S-ATTN mechanism. In the latter case, we rely only on the agent’s local state s_i^t to sequentially update the RNN hidden state \mathbf{q}_i^t of the observation encoder after it has been initialized using our M-ATTN mechanism. Our S-ATTN mechanism pays attention to the stopped car in front of the target vehicle and helps the model to make predictions that are compliant with human driving behavior. Note how the predictive trajectory distribution accurately captures the motion pattern of the target vehicle that slows down to avoid colliding with its neighbor as opposed to when no social attention is used.

To highlight how our unified observation encoding scheme (Section III-C) helps the model make accurate predictions, we consider three urban traffic examples. In Fig. 1, we visualize the corresponding activation maps of the map encoder obtained using the GradCAM technique [31] along with the social attention weights of the perceived neighbors. In the first example, the model focuses on the challenging intersection area around the target vehicle and pays high attention to the leading car along its lane. In the second example, the most salient map area is the crosswalk (light red polygons) in front of the target vehicle, where a number of agents are waiting for the traffic lights to turn green. Hence, the vehicle’s attention focuses on these neighbors while ignoring irrelevant agents such as the three stopped cars on the outer right lane. In the third example, the target vehicle is static and the model relies only on the observed neighbors’ states to make predictions with little attention paid to the map. These examples demonstrate that our approach can flexibly utilize the environmental map information and the agents social states to make predictions.

We refer to the supplementary material and video for additional examples and results on all three tested datasets.

V. CONCLUSION

We have introduced ContextVAE, a fast and lightweight approach for context-aware vehicle trajectory prediction. ContextVAE relies on a timewise VAE architecture and employs a map encoding module that performs observation encoding in a unified and socially-aware way. We show that our approach provides high-fidelity, map-compliant predictions on a variety of heterogeneous datasets, capturing the multi-modal nature of vehicle motions and their interactions with neighbor agents. We note that the model performance can be further improved by leveraging post-processing techniques like final position clustering [4] and bootstrap aggregation [32], at the cost of higher running times. An interesting avenue for future work is to account for dynamic environmental information like traffic lights in the observation encoding scheme by introducing local maps timewise. It is also worth exploring how map representation influences context encoding and model performance, including trying alternative ways of map rasterization and using vectorized road graphs to capture contextual features.

REFERENCES

- [1] H. Caesar, V. Bankiti, A. H. Lang, S. Vora, V. E. Liong, Q. Xu, A. Krishnan, Y. Pan, G. Baldan, and O. Beijbom, “nuscenes: A multimodal dataset for autonomous driving,” in *IEEE/CVF Conference on Computer Vision and Pattern Recognition*, 2020, pp. 11 621–11 631.
- [2] J. Houston, G. Zuidhof, L. Bergamini, Y. Ye, L. Chen, A. Jain, S. Omari, V. Iglovikov, and P. Ondruska, “One thousand and one hours: Self-driving motion prediction dataset,” in *Conference on Robot Learning*, 2021, pp. 409–418.
- [3] S. Ettinger, S. Cheng, B. Caine, C. Liu, H. Zhao, S. Pradhan, Y. Chai, B. Sapp, C. R. Qi, Y. Zhou, Z. Yang, A. Chouard, P. Sun, J. Ngiam, V. Vasudevan, A. McCauley, J. Shlens, and D. Anguelov, “Large scale interactive motion forecasting for autonomous driving: The Waymo open motion dataset,” in *IEEE/CVF International Conference on Computer Vision*, 2021, pp. 9710–9719.
- [4] P. Xu, J.-B. Hayet, and I. Karamouzas, “SocialVAE: Human trajectory prediction using timewise latents,” in *European Conference on Computer Vision*. Springer, 2022.
- [5] J. L. V. Espinoza, A. Liniger, W. Schwarting, D. Rus, and L. Van Gool, “Deep interactive motion prediction and planning: Playing games with motion prediction models,” in *Learning for Dynamics and Control Conference*, 2022, pp. 1006–1019.
- [6] T. Salzmann, B. Ivanovic, P. Chakravarty, and M. Pavone, “Trajectron++: Dynamically-feasible trajectory forecasting with heterogeneous data,” in *European Conference on Computer Vision*, 2020, pp. 683–700.
- [7] Y. Yao, E. Atkins, M. Johnson-Roberson, R. Vasudevan, and X. Du, “Bi-TraP: Bi-directional pedestrian trajectory prediction with multi-modal goal estimation,” *IEEE Robotics and Automation Letters*, vol. 6, no. 2, pp. 1463–1470, 2021.
- [8] A. Sadeghian, V. Kosaraju, A. Sadeghian, N. Hirose, H. Rezatofighi, and S. Savarese, “SoPhie: An attentive GAN for predicting paths compliant to social and physical constraints,” in *IEEE/CVF Conference on Computer Vision and Pattern Recognition*, 2019, pp. 1349–1358.
- [9] T. Phan-Minh, E. C. Grigore, F. A. Boulton, O. Beijbom, and E. M. Wolff, “CoverNet: Multimodal behavior prediction using trajectory sets,” in *Proceedings of the IEEE/CVF Conference on Computer Vision and Pattern Recognition*, 2020, pp. 14 074–14 083.
- [10] S. Konev, K. Brodt, and A. Sanakoyeu, “MotionCNN: A strong baseline for motion prediction in autonomous driving,” in *Proc. of the IEEE/CVF Conference on Computer Vision and Pattern Recognition Workshops*, 2021.
- [11] Y. Chai, B. Sapp, M. Bansal, and D. Anguelov, “Multipath: Multiple probabilistic anchor trajectory hypotheses for behavior prediction,” *arXiv preprint arXiv:1910.05449*, 2019.
- [12] H. Cui, V. Radosavljevic, F.-C. Chou, T.-H. Lin, T. Nguyen, T.-K. Huang, J. Schneider, and N. Djuric, “Multimodal trajectory predictions for autonomous driving using deep convolutional networks,” in *IEEE International Conference on Robotics and Automation*, 2019, pp. 2090–2096.
- [13] N. Deo and M. M. Trivedi, “Trajectory forecasts in unknown environments conditioned on grid-based plans,” *arXiv preprint arXiv:2001.00735*, 2020.
- [14] R. Girgis, F. Golemo, F. Codevilla, M. Weiss, J. A. D’Souza, S. E. Kahou, F. Heide, and C. Pal, “Latent variable sequential set transformers for joint multi-agent motion prediction,” in *International Conference on Learning Representations*, 2021.
- [15] L. Zhang, P.-H. Su, J. Hoang, G. C. Haynes, and M. Marchetti-Bowick, “Map-adaptive goal-based trajectory prediction,” in *Conference on Robot Learning*, 2021, pp. 1371–1383.
- [16] X. Huang, S. G. McGill, J. A. DeCastro, L. Fletcher, J. J. Leonard, B. C. Williams, and G. Rosman, “DiversityGAN: Diversity-aware vehicle motion prediction via latent semantic sampling,” *IEEE Robotics and Automation Letters*, vol. 5, no. 4, pp. 5089–5096, 2020.
- [17] C. Wang, Y. Wang, M. Xu, and D. Crandall, “Stepwise goal-driven networks for trajectory prediction,” *IEEE Robotics and Automation Letters*, 2022.
- [18] J. Gao, C. Sun, H. Zhao, Y. Shen, D. Anguelov, C. Li, and C. Schmid, “VectorNet: Encoding HD maps and agent dynamics from vectorized representation,” in *IEEE/CVF Conference on Computer Vision and Pattern Recognition*, 2020, pp. 11 525–11 533.
- [19] M. Liang, B. Yang, R. Hu, Y. Chen, R. Liao, S. Feng, and R. Urtasun, “Learning lane graph representations for motion forecasting,” in *European Conference on Computer Vision*. Springer, 2020, pp. 541–556.
- [20] S. Khandelwal, W. Qi, J. Singh, A. Hartnett, and D. Ramanan, “What-if motion prediction for autonomous driving,” *arXiv preprint arXiv:2008.10587*, 2020.
- [21] B. Kim, S. H. Park, S. Lee, E. Khoshimjonov, D. Kum, J. Kim, J. S. Kim, and J. W. Choi, “LaPred: Lane-aware prediction of multi-modal future trajectories of dynamic agents,” in *IEEE/CVF Conference on Computer Vision and Pattern Recognition*, 2021, pp. 14 636–14 645.
- [22] C. Luo, L. Sun, D. Dabiri, and A. Yuille, “Probabilistic multi-modal trajectory prediction with lane attention for autonomous vehicles,” in *IEEE/RSJ International Conference on Intelligent Robots and Systems*, 2020, pp. 2370–2376.
- [23] H. Zhao, J. Gao, T. Lan, C. Sun, B. Sapp, B. Varadarajan, Y. Shen, Y. Shen, Y. Chai, C. Schmid *et al.*, “TNT: Target-driven trajectory prediction,” in *Conference on Robot Learning*, 2021, pp. 895–904.
- [24] Q. Sun, X. Huang, J. Gu, B. C. Williams, and H. Zhao, “M2I: From factored marginal trajectory prediction to interactive prediction,” in *Proc. of the IEEE/CVF Conference on Computer Vision and Pattern Recognition*, 2022, pp. 6543–6552.
- [25] N. Deo, E. Wolff, and O. Beijbom, “Multimodal trajectory prediction conditioned on lane-graph traversals,” in *5th Annual Conference on Robot Learning*, 2021.
- [26] S. Casas, C. Gulino, S. Suo, and R. Urtasun, “The importance of prior knowledge in precise multimodal prediction,” in *IEEE/RSJ International Conference on Intelligent Robots and Systems*, 2020, pp. 2295–2302.
- [27] W. Zeng, M. Liang, R. Liao, and R. Urtasun, “LaneRCNN: Distributed representations for graph-centric motion forecasting,” in *IEEE/RSJ International Conference on Intelligent Robots and Systems*, 2021, pp. 532–539.
- [28] T. Gilles, S. Sabatini, D. Tsishkou, B. Stanculescu, and F. Moutarde, “Gohome: Graph-oriented heatmap output for future motion estimation,” in *IEEE International Conference on Robotics and Automation*, 2022, pp. 9107–9114.
- [29] J. Amirian, J.-B. Hayet, and J. Pettré, “Social Ways: Learning multi-modal distributions of pedestrian trajectories with GANs,” in *Proceedings of the IEEE/CVF Conference on Computer Vision and Pattern Recognition Workshops*, 2019.
- [30] J. Ngiam, V. Vasudevan, B. Caine, Z. Zhang, H.-T. L. Chiang, J. Ling, R. Roelofs, A. Bewley, C. Liu, A. Venugopal *et al.*, “Scene Transformer: A unified architecture for predicting future trajectories of multiple agents,” in *International Conference on Learning Representations*, 2021.
- [31] R. R. Selvaraju, M. Cogswell, A. Das, R. Vedantam, D. Parikh, and D. Batra, “Grad-CAM: Visual explanations from deep networks via gradient-based localization,” in *IEEE International Conference on Computer Vision*, 2017, pp. 618–626.
- [32] B. Varadarajan, A. Hefny, A. Srivastava, K. S. Refaat, N. Nayakanti, A. Corrman, K. Chen, B. Douillard, C. P. Lam, D. Anguelov *et al.*, “Multipath++: Efficient information fusion and trajectory aggregation for behavior prediction,” in *IEEE International Conference on Robotics and Automation*, 2022, pp. 7814–7821.

Context-Aware Timewise VAEs for Real-Time Vehicle Trajectory Prediction – Supplementary Material

Pei Xu, Jean-Bernard Hayet and Ioannis Karamouzas

TABLE S1
PREDICTION ERRORS WITH DIFFERENT CNN MODULES FOR MAP FEATURE EXTRACTION.

CNN Module	Infer. Time	# of Params.	<i>nuScenes</i>				<i>Lyft</i>				<i>Waymo</i>			
			minADE _k		minFDE _k		minADE _k		minFDE _k		minADE _k		minFDE _k	
			k = 1	k = 5	k = 1	k = 5	k = 1	k = 5	k = 1	k = 5	k = 1	k = 5	k = 1	k = 5
ResNet18	0.23s	11.7M	3.543	1.586	8.244	3.277	0.247	0.165	0.548	0.324	0.600	0.306	1.532	0.709
ResNet34	0.42s	21.8M	3.767	1.727	8.842	3.640	0.248	0.165	0.553	0.325	0.600	0.306	1.536	0.706
ResNet50	0.56s	25.6M	3.717	1.711	8.811	3.628	0.247	0.164	0.550	0.323	0.599	0.305	1.530	0.705
ResNet101	0.93s	44.5M	3.669	1.655	8.653	3.463	0.246	0.164	0.545	0.323	0.603	0.307	1.543	0.703
ResNet152	1.33s	60.2M	3.728	1.728	8.773	3.657	0.244	0.164	0.544	0.321	0.598	0.306	1.530	0.708
EfficientNet-B0	0.25s	5.3M	3.715	1.740	8.733	3.676	0.246	0.165	0.548	0.325	0.585	0.299	1.491	0.686
EfficientNet-B1	0.32s	7.8M	3.864	1.826	9.199	3.947	0.247	0.165	0.550	0.328	0.587	0.300	1.493	0.688
EfficientNet-B2	0.35s	9.1M	3.765	1.726	8.870	3.657	0.246	0.164	0.547	0.322	0.590	0.301	1.501	0.692
EfficientNet-B3	0.44s	12.2M	3.840	1.785	9.027	3.837	0.247	0.165	0.548	0.326	0.593	0.301	1.511	0.692
MobileNet-V2	0.20s	3.5M	3.780	1.738	8.888	3.671	0.251	0.165	0.560	0.321	0.585	0.298	1.492	0.684
MobileNet-V3-Small	0.10s	2.5M	3.817	1.768	8.964	3.794	0.250	0.165	0.558	0.324	0.592	0.302	1.508	0.695
MobileNet-V3-Large	0.17s	5.5M	3.650	1.767	8.606	3.749	0.246	0.164	0.548	0.323	0.594	0.304	1.515	0.700

TABLE S2
PREDICTION ERRORS WITH VARYING PREDICTION HORIZON.

Prediction Horizon	<i>nuScenes</i>				<i>Lyft</i>				<i>Waymo</i>			
	minADE _k		minFDE _k		minADE _k		minFDE _k		minADE _k		minFDE _k	
	k = 1	k = 5	k = 1	k = 5	k = 1	k = 5	k = 1	k = 5	k = 1	k = 5	k = 1	k = 5
3s	1.36	0.64	2.71	1.10	0.24	0.16	0.54	0.32	0.59	0.30	1.49	0.68
4s	1.98	0.91	4.26	1.69	0.30	0.19	0.72	0.41	1.01	0.51	2.70	1.18
5s	2.71	1.22	6.11	2.42	0.43	0.27	1.10	0.61	1.52	0.72	4.12	1.75
6s	3.54	1.59	8.24	3.28	0.58	0.37	1.60	0.88	2.11	1.02	5.81	2.43

TABLE S3
ABLATION STUDIES.

S-ATTN	MAP	M-ATTN	<i>nuScenes</i>				<i>Lyft</i>				<i>Waymo</i>			
			minADE _k		minFDE _k		minADE _k		minFDE _k		minADE _k		minFDE _k	
			k = 1	k = 5	k = 1	k = 5	k = 1	k = 5	k = 1	k = 5	k = 1	k = 5	k = 1	k = 5
-	-	-	3.75	2.30	8.80	5.03	0.28	0.20	0.64	0.39	0.68	0.45	1.78	1.11
✓	-	-	3.69	2.21	8.76	5.03	0.27	0.19	0.61	0.38	0.65	0.43	1.71	1.06
✓	Indie	-	3.66	1.82	8.49	4.10	0.26	0.17	0.60	0.35	0.63	0.37	1.68	0.85
✓	Integrated	-	3.61	1.79	8.30	3.87	0.26	0.17	0.58	0.32	0.62	0.33	1.65	0.70
✓	Integrated	✓	3.54	1.59	8.24	3.28	0.24	0.16	0.54	0.32	0.59	0.30	1.49	0.68

I. SEMANTIC MAP RASTERIZATION

We use a rasterized, 224×224 local semantic map with a 1:1 ratio between pixels and world coordinates in meters. We refer to Fig. 3 for examples of the rasterized semantic maps used in each test dataset. Because each dataset has its own map data format, the semantic maps used for each model are

Pei Xu and Ioannis Karamouzas are with the School of Computing at Clemson University, South Carolina, USA. {peix, ioannis}@clemson.edu

Jean-Bernard Hayet is with the Department of Computer Science at CIMAT, A.C., Mexico. jbhayet@cimat.mx

somewhat different. In *nuScenes* and *Lyft*, the 1st and 2nd channels contain the road divider and lane divider, respectively. The 3rd channel of the *nuScenes* maps consists of the drivable area and the pedestrian crosswalks, obtained through the map API. The drivable area covers lane regions plus some off-road regions where vehicles can move. For *Lyft*, there is no drivable area provided directly by its map API. As such, we draw the drivable areas by filling the provided boundaries of each lane segment. Similarly, *Waymo* provides only road edges as a collection of single lines without the boundary information defined for lane segments. We, therefore, draw the lane center

TABLE S4
SENSITIVITY ANALYSIS OF MAP ENCODING MODULES ON OTHER VAE MODELS.

	<i>nuScenes</i>				<i>Lyft</i>				<i>Waymo</i>			
	minADE _k		minFDE _k		minADE _k		minFDE _k		minADE _k		minFDE _k	
	<i>k</i> = 1	<i>k</i> = 5	<i>k</i> = 1	<i>k</i> = 5	<i>k</i> = 1	<i>k</i> = 5	<i>k</i> = 1	<i>k</i> = 5	<i>k</i> = 1	<i>k</i> = 5	<i>k</i> = 1	<i>k</i> = 5
Trajectron++ (No map)	3.97	2.50	9.24	5.89	0.37	0.31	0.88	0.62	0.88	0.70	2.37	1.60
Trajectron++ (Indie)	4.08	2.41	9.67	5.63	0.38	0.26	0.89	0.57	0.88	0.56	2.37	1.41
Trajectron++ (Integrated)	3.88	2.40	9.17	5.21	0.30	0.21	0.78	0.49	0.85	0.52	2.21	1.11
BiTraP (No map)	4.10	2.50	9.71	5.90	0.36	0.31	0.83	0.61	0.88	0.62	2.36	1.55
BiTraP (Indie)	4.10	2.40	9.70	5.60	0.36	0.25	0.83	0.55	0.88	0.55	2.35	1.40
BiTraP (Integrated)	3.87	2.40	9.15	5.17	0.30	0.20	0.69	0.40	0.85	0.52	2.20	1.10

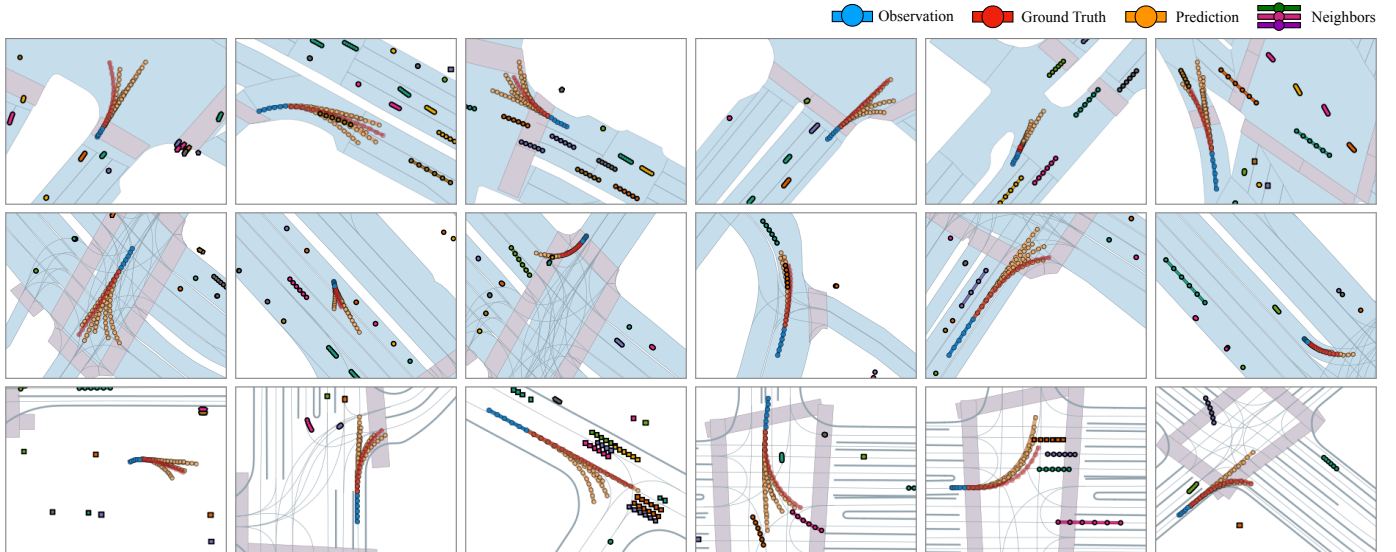


Fig. S1. Examples of ContextVAE predictions on *nuScenes*, *Lyft* and *Waymo* datasets, from top to bottom.

lines across all channels to enhance the representation of drivable areas. Road dividers and edges are drawn on the 1st and 2nd channels respectively, with the crosswalk regions still on the 3rd channel.

II. ADDITIONAL RESULTS

A. Sensitivity Analysis

a) *CNN Modules*: Table S1 shows the model performance when different CNN modules are employed for map feature extraction. Overall, there are no significant differences across all the tested CNN modules on large *Lyft* and *Waymo* datasets. Thus, a small module like MobileNet-V2 or EfficientNet-B0 can be safely used. For *nuScenes*, there is a larger error variance between the different CNN modules with the efficient ResNet18 providing the best performance.

b) *Prediction Horizon*: We analyze the effect that different prediction horizons have on the performance of ContextVAE. We optimize each tested model using the corresponding horizon and report the corresponding minADE/minFDE performance in Table S2.

c) *Ablation Study*: In Table S3, we report the full ablation study results of ContextVAE on all three datasets. The studied components are the same as the ablation study in the main text (cf. Section IV.C). As can be seen, our proposed

unified observation scheme that leverages a dual attention mechanism leads to the best performance on all tested datasets.

B. Integrated vs. Independent Maps for Observation Encoding

Following the analysis in Section IV-D, in Table S4, we report the performance of Trajectron++ [1] and BiTraP [2] when different map integration schemes are employed. Both approaches leverage the same RNN-based observation encoder and employ the same conditional VAE backbone proposed in [1]. When no map is used, the models rely only on the social attention mechanism of Trajectron++. We note that, as opposed to the S-ATTN block of ContextVAE, the social attention of Trajectron++ accounts for the agent's and its neighbors' local states without leveraging any social features. Similar to our ablation studies, when using Indie maps, the observation encoder only accounts for the agent's states and its output \mathbf{q}_t^i is concatenated with the extracted map features \mathbf{M}_i^1 before it is passed to the VAE decoder. When Integrated maps are used, we use the map features to initialize the observation encoder, i.e. $\mathbf{q}_i^1 = \text{CONCAT}(\mathbf{M}_i^1, \sum_j f_{n^1}(\{\mathbf{n}_{j|i}\}))$. In both approaches, we use the default map encoding module from Trajectron++ to perform feature extraction. As can be seen in the table, the introduction of Indie maps slightly improves the multimodal performance ($k = 5$) over models that do not rely on semantic

maps. However, there is no evident improvement on the most likely, deterministic prediction ($k = 1$). This is consistent with the ablation study results reported in [1]. Using Integrated maps, however, can bring effective improvements to both deterministic and multimodal predictions in all the tested datasets.

III. CASE STUDIES

In Fig. S1, we show additional examples of our approach on the three tested datasets. We refer to the supplementary video for related results.

REFERENCES

- [1] T. Salzmann, B. Ivanovic, P. Chakravarty, and M. Pavone, “Trajectron++: Dynamically-feasible trajectory forecasting with heterogeneous data,” in *European Conference on Computer Vision*, 2020, pp. 683–700.
- [2] Y. Yao, E. Atkins, M. Johnson-Roberson, R. Vasudevan, and X. Du, “BiTraP: Bi-directional pedestrian trajectory prediction with multi-modal goal estimation,” *IEEE Robotics and Automation Letters*, vol. 6, no. 2, pp. 1463–1470, 2021.